Available online at www.sciencedirect.com
SCIENCE DIRECT®
International Journal of Heat and Mass Transfer 49 (2006) 2877–2888
International Journal of HEAT and MASS TRANSFER
www.elsevier.com/locate/ijhmt

Maximum heat flux in relation to quenching of a high temperature surface with liquid jet impingement

Aloke Kumar Mozumder, Masanori Monde *, Peter Lloyd Woodfield, Md. Ashraful Islam

Department of Mechanical Engineering, Saga University, 1 Honjo-machi, Saga 840-8502, Japan

Received 20 June 2005
Available online 17 April 2006

Abstract

Experimental investigation has been conducted for quenching of hot cylindrical blocks made of copper, brass and steel with initial block temperature 250–400 °C by a subcooled water jet of diameter of 2 mm. The subcooling was from 5 to 80 K and the jet velocity was from 3 to 15 m/s. After impingement, the jet stagnates for a certain period of time in a small region near the centre and then the wetting front starts moving outwards. During this movement, when the surface temperature at the wetting front drops to 120–200 °C, the surface heat flux reaches its maximum value due to forced convection nucleation boiling. The maximum heat flux is a strong function of the position on the hot surface, jet velocity, block material properties and jet subcooling. A new correlation for maximum heat flux is proposed.

Keywords: Quenching; Wetting front; Inverse solution; Impinging jet; Boiling curve

1. Introduction

Jet impingement quenching is used widely in industry. At present, mainly two interest groups are dealing with the research and development of jet quenching. One group is interested to use the knowledge of quenching for controlling the mechanical and metallurgical properties of industrial products. They also use this knowledge for controlling high temperature in manufacturing industries. The other interest group uses jet impingement quench cooling to prevent overheating. For the purpose of emergency core cooling of nuclear reactor, water jets are impinged on the hot fuel element and the heat flux is the vital parameter at that time. Impinging jet cooling is also in use for removal of heat from electronic chips.

Quenching can be defined as a heat transfer process in which extremely rapid cooling results from bringing a high temperature solid into sudden contact with a lower temperature fluid. Studies of jet impingement quenching have been performed by a number of researchers [1–4] who gave attention to heat flux, temperature, and the flow field by flow visualization. Some other researchers [5,6] have focused on the phenomena that occurred during quenching of a hot surface.

Knowledge of the maximum heat flux and its position is of great importance since the maximum heat flux usually corresponds to the maximum temperature gradient in the solid and therefore the largest thermal stress. In addition the maximum cooling rate is directly connected to the maximum heat flux. Thus to be able to predict and ultimately control the maximum heat flux during quenching is a key goal for boiling research.

In the present article we have decided to use the term 'maximum heat flux' rather than 'critical heat flux' (CHF) since there may be a difference between the critical heat flux appearing in steady-state experiments and the maximum heat flux arising in quench cooling experiments. There is a wealth of literature relating to steady-state critical heat flux [7] but in contrast relatively fewer

* Corresponding author. Tel.: +81 952 28 8608; fax: +81 952 28 8587.
E-mail addresses: 03ts11@edu.cc.saga-u.ac.jp (A.K. Mozumder), monde@me.saga-u.ac.jp (M. Monde), peter@me.saga-u.ac.jp (P.L. Woodfield), ashraful@me.saga-u.ac.jp (M.A. Islam).

0017-9310/$ - see front matter © 2006 Elsevier Ltd. All rights reserved.
doi:10.1016/j.ijheatmasstransfer.2006.01.048

Nomenclature

a	thermal diffusivity (m^2/s)
c	specific heat (kJ/kg K)
d	diameter of liquid jet (mm)
D	diameter of heated surface (mm)
h_{fg}	latent heat of evaporation (J/kg)
Ja	Jacob number $= (\rho_l/\rho_g)(c_l\Delta T_{sub}/h_{fg})$
q_c	critical heat flux of subcooled liquid jet (MW/m^2)
q_{co}	critical heat flux of saturated liquid jet (MW/m^2)
q_{max}	maximum heat flux (MW/m^2)
q_w	surface heat flux (MW/m^2)
r	position in the radial direction of the block (mm)
r_q	radial position at q_{max} (mm)
t	time (counted from the impingment of jet) (s)
T	measured temperature (°C)
T_b	block initial temperature (°C)
T_{liq}	liquid temperature (°C)
T_{sat}	saturated temperature of liquid (°C)
T_w	surface temperature (°C)
u	jet velocity (m/s)

Greek symbols

ΔT_{sub}	liquid subcooling (K)
λ	thermal conductivity (W/mK)
ρ	density (kg/m^3)
σ	surface tension (N/m)

Subscripts

g	gas (vapor)
l	liquid
s	solid

publications are available for insight into maximum heat flux during transient quenching [8–16].

Barnea and Elias [9] conducted experiments and performed a theoretical study of flow and heat transfer regimes during quenching of a heated vertical channel. They observed that the quench front was in the transition-boiling region, which stretched between the dry and wet segments of the surface. Dua and Tien [10] performed an experimental study on rewetting of a copper tube by a falling film of liquid nitrogen. They observed that the maximum heat flux in rewetting occurred at the location of the wet front and its magnitude was comparable to the average of the maximum and the minimum heat fluxes of nucleate and film pool boiling.

Filipovic et al. [11] performed transient boiling experiments using a large preheated test specimen exposed to a water wall jet on its top surface. They reported that during much of the quenching process, conditions on the test surface were characterized by propagation of a quench front in the direction of flow along the surface. Heat transfer occurred by nucleate boiling or single-phase convection upstream of the front, while film boiling existed in a precursory region downstream of the front. The front itself was at the leading edge of a transition-boiling zone, which was approximately coincident with location of maximum heat flux. They also found that the location of the maximum heat flux on the surface moved downstream with increasing time and its value decreased with time. Kumagai and Suzuki [12] also conducted a transient cooling experiment of a hot metal slab but with an impinging plane jet. They observed that local surface temperature fell rapidly when the temperature at that point reached the temperature corresponding to the high heat flux region of transition boiling.

Hall et al. [13] performed an experimental study of boiling heat transfer during quenching of a cylindrical copper disk by a subcooled, circular, free-surface water jet. Their study reveals that quenching measurements encompass three distinct boiling regimes; nucleate boiling in the impingement zone, the upper limit of nucleate boiling (maximum heat flux for the entire surface) and transition boiling which is characterized by minimum film boiling heat flux and the temperatures for the radial flow region. They correlated the radial distributions of maximum heat flux data with relations developed by others researchers from steady-state experiments for radial flow region.

Hammad et al. [14] conducted experiments for investigating the heat transfer characteristics and wetting front during quenching of a high temperature cylindrical block by water jet at atmospheric pressure. Ochi et al. [16] also experimentally investigated transient heat transfer using circular water jet impingement. Their test piece was a flat plate. They observed that heat flux at the stagnation point (in the central region) was higher than those at further radial positions. In the stagnation region the heat flux increases with water subcooling and with jet velocity divided by the nozzle diameter. Their observation revealed that the velocity of the rewetting front increases with nozzle diameter, jet velocity and water subcooling.

In quenching experiments on large test pieces a phenomenon termed 'wetting front' [14], 'quench front' [9] or 'wet-front' [10] has been observed. It is a little difficult to unambiguously define what the 'wetting front' is. The wetting front phenomenon should not be thought of as a single point or line but the entire transition boiling region should be understood to be a part of the wetting front. However, for convenience of discussion, in the present article the wetting front is defined as follows. In all of our experiments, a black region at the outer zone of the moving liquid was

observed on the basis of the video images. The wetting front is defined as the visible outer edge of this black region in the present study. Most of the time, an inner edge of this black region is also visible as shown in the Fig. 3. A complete thermal and hydrodynamic criterion for this moving wetting front has not yet been clarified.

The position and magnitude of maximum heat flux are among the important criteria for understanding the quenching phenomena. The aims of the present study are to investigate the parameters that control the position of maximum heat flux and to predict its magnitude as a function of experimental parameters. The parameters like initial block temperature, jet velocity, liquid subcooling and block material properties are considered predominantly in this study. Correlations for maximum heat flux are also proposed in this study.

2. Experimental apparatus and procedure

The major components of the experimental set-up for the present study are a cylindrical block, a data acquisition system, a fluid flow system and a high-speed video camera. The test block (1) as shown in the Fig. 1 is uniformly heated to the desired initial temperature by using three types of electrical heaters (16) mounted on the top and around the block. The velocity of the liquid jet is adjusted by a regulating valve. To protect the test surface from oxidation, an inert atmosphere is maintained by feeding nitrogen gas from a cylinder (14). The whole experiment is conducted at atmospheric pressure. The liquid tank (11) is filled with distilled water at first up to the same level for each experiment, which is ensured by viewing through the level gauge (10). A pump (7) located at the bottom of the set-up is used for pumping the distilled water through

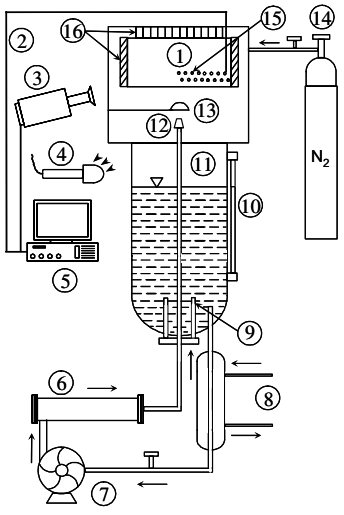

Fig. 1. Schematic diagram of the experimental set-up: (1) Tested block; (2) Thermocouple wire; (3) High-speed video camera; (4) Microphone; (5) Data acquisition system; (6) Auxiliary heater; (7) Pump; (8) Cooler, (9) Main heater; (10) Level gauge; (11) Liquid tank; (12) Nozzle; (13) Rotary shutter; (14) Nitrogen cylinder; (15) Thermocouple positions; (16) Block heater.

Table 1
Experimental conditions of the present study

Block material	Initial temperature, T_b [°C]	Jet velocity, u [m/s]	Jet sub-cooling, ΔT_{sub} [K]
Copper, Brass, Steel	400, 350, 300, 250	15, 10, 5, 3	80, 50, 20, 5

a nozzle (12) of diameter 2 mm, which is set centrally 44 mm from the test surface. A shutter (13) is mounted in front of the nozzle to prevent water from striking the block (1) prematurely and to maintain a constant water temperature by forcing it to run within a closed loop system. The desired temperature of the water is obtained by controlling the main heater (9), auxiliary heater (6) or cooled by a cooler (8). A dynamic strain meter is attached at two points of the flow line before the nozzle for measuring differential pressure from which jet velocity is calculated and this velocity is adjusted by a regulating valve.

After fulfilling the desired experimental conditions, the shutter is opened so that the water jet strikes on the centre of the heated surface. A high-speed video camera (3) is employed to capture the video images of flow pattern during quenching and simultaneously a microphone (4) is used to measure the noise level. Sixteen thermocouples (15) measure the temperatures inside the heated block with the help of the data acquisition system (5).

Table 1 shows all the experimental conditions employed in the present study. During the experiment, ±2 °C deviation from the desired initial block temperature was allowed. The accuracy of the jet velocity was ±0.1 m/s. Before starting the experiment, the initial temperature of the liquid could be controlled to within 1 °C from the set point. But for long cooling experimental conditions, during the experimental run, it was difficult to maintain the initial liquid temperature. It was noticed sometimes ±2 °C variation from the initial temperature of the liquid.

2.1. Heated block

The heated block is 94 mm in diameter and 59 mm in height with cylindrical shape. For inserting the thermocouples, a small section of the block was made removable [15] but no cuts were made through the test surface itself. The effect of this cutting is limited to one corner of the block in an area having radius more than 30 mm, it is found from video observation that there is a departure from symmetry in the expanding of the wetting front. For this reason, all data reported in this study are for radial positions less than 30 mm where the results may be considered axisymmetric. Sixteen thermocouples (CA-type, 1 mm sheath diameter and 0.1 mm wire diameter) are located at two different depths, 2.1 mm and 5 mm from the surface as described elsewhere [15]. Eight thermocouples are inserted along the radial direction at each depth. For the depth 2.1 mm, the eight thermocouples are located sequentially with a 5 mm interval and starting from a radial position 6.5 mm. For the depth 5.0 mm, the other eight thermocouples start

from radial position 4 mm and are sequentially spaced with the same interval of 5 mm. For maintaining an inert atmosphere (to protect the heated test surface from oxidation), the surface was plated with a thin layer of gold with 16 μm thickness, which has an excellent oxidation resistance and also a good thermal conductivity; $\lambda \approx 317$ W/mK. After conducting a huge number of experiments with same block, a portion of the gold layer removed away from the test surface. No significant difference on q_{max} value was observed due to this small change of the surface coating. The surface roughness is 0.2–0.4 μm. The block is mainly heated with a 0.94 kW coil heater mounted around it. For maintaining a uniform heat flux from the test surface two auxiliary heaters are used; one of them is of band type, 0.65 kW, and is set around the block circumference, while the second is of slot type, 0.5 kW, and is placed in the four groves in the upper part of the block.

2.2. Data acquisition system

The data acquisition system scanned the signal from the thermocouples sequentially at 0.05-s intervals, with 8.0 ms needed to read all of the thermocouples using an analog–digital (AD) converter with 16-bit resolution. The uncertainty for the measurement of the temperature is ±0.1 °C, while the uncertainty in the placement of the thermocouples is estimated to be ±0.1 mm. The estimated time lag for the response of the thermocouple is less than 0.1 s.

2.3. Visual observation system

A high-speed video camera with a maximum resolution of 1280 × 1024 pixels and a maximum rate of 10,000 frame/s was employed during quenching. From individual frames of the video images, the flow pattern, the wetting front movement and the splattering of liquid droplets were analyzed.

2.4. Analysis of the experimental data

Temperatures were measured beneath the hot surface inside the block on which jet was impinged. These temperatures were then used to estimate the surface temperature and surface heat flux because it was impossible to measure the surface temperature directly during quenching. A two-dimensional inverse solution for heat conduction adopted from Monde et al. [17] and Hammad et al. [18] was applied for estimating the surface parameters based on the measured temperature. Temperature was measured at eight different locations for each particular depth inside block. To improve the space resolution of the calculation procedure [19] additional points were interpolated between the measured points taking into account time and space trends in the data, so that the number of reference points was increased from 8 to 29. Some improvements to implementation of the inverse calculation procedure suggested by Woodfield et al. [19] were incorporated also. The procedure for estimation of surface temperature and surface heat flux from inverse solution has been described in Appendix A. It is worth mentioning here that the values of material thermal properties such as density, specific heat and conductivity used in the inverse solution have been taken at 250 °C. The experimental range for initial block temperature used in the present study is 250–400 °C as given in Table 1. No significant changes due to material properties are expected within this temperature range.

In the present work the closest thermocouple to the centerline of the test piece was at a radial position of 4 mm. Thus only results for a radial position greater than about 5 mm are reported in this study.

3. Results and discussion

3.1. Cooling curve and heat flux

An example of the surface temperature and heat flux distributions with time and radial position estimated from the inverse solution is presented in Fig. 2. For many conditions, after the jet first strikes the hot surface, the wetting region stays for a while in a small region near the center before wetting the entire surface. This wetting delay has been defined as the resident time by Mozumder et al. [20] where cooling curves have been categorized in three types: long resident time, moderate resident time and short resident time. Fig. 2 is a representative plot of short resident time conditions where the wetting front starts moving almost immediately after the first striking of the jet.

The cooling curve in Fig. 2 shows that the temperature close to the center of the test piece drops from 400 to 100 °C within 2 s after the jet first strikes. During this time, the heat flux increases drastically and reaches its maximum value. It takes about 10 s for the outer radial positions to come to the temperature 100 °C. The peak in the heat flux curve moves outwards in the radial direction as the liquid wets the surface. After 10 s, there is almost no variation of radial temperature distribution and the overall surface temperature of the block comes to around 80 °C. Finally the surface temperature drops gradually and slowly.

Focusing on the beginning of the cooling curve, it is notable that the surface temperature nearer the center drops by as much as 300 °C during the first few seconds. This sudden drop is partly due to a localized transient heat conduction response on the contact of the solid and water to the large step change in heat flux when the jet strikes the surface [20]. However, for the case shown in Fig. 2, the drop is more than this initial transient effect since as the temperature falls, the heat flux near the center simultaneously increases resulting in the very large change in surface temperature.

The key feature of the heat flux distribution in Fig. 2 is the moving of the maximum heat flux point. The rapid drop in temperature evident in the cooling curves is a direct result of the movement of the maximum heat flux point. For the experimental condition shown in the Fig. 2, the heat flux is much less than 1 MW/m^2 before the movement

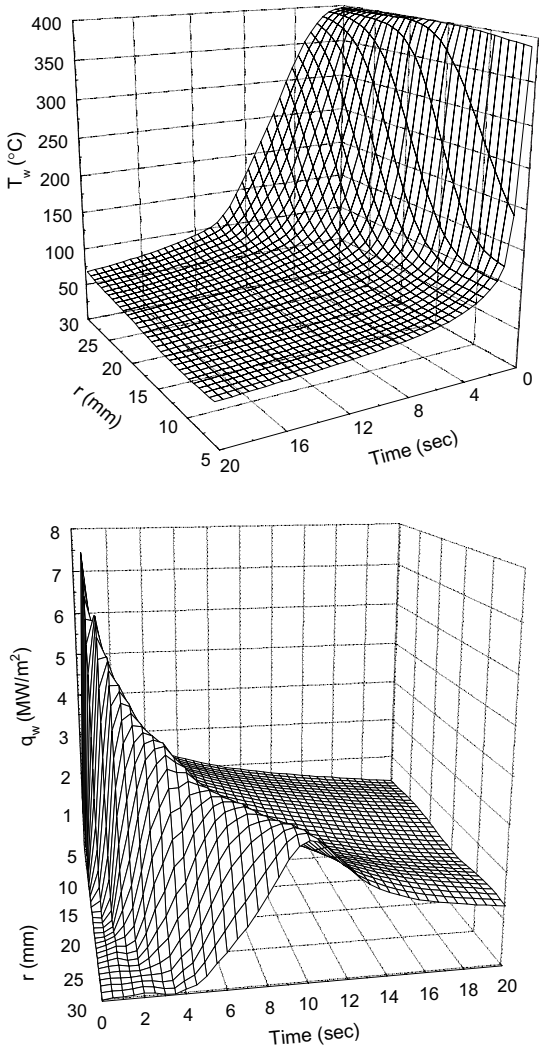

Fig. 2. Cooling curve and heat flux distribution during quenching for brass ($T_b = 400$ °C, $\Delta T_{sub} = 80$ K, $u = 15$ m/s).

of the wetting front. When the wetting front starts moving, the heat flux 5 mm from the center reaches about 7.5 MW/m^2. This kind of trend was observed for many of the experiment conditions for this study. Generally the heat flux after the wetting front begins moving was found to be in the range of 5–60 times higher than before movement especially for slow cooling conditions (low sub-cooling and smaller jet velocity conditions). It should be mentioned here that the heat flux before the movement of the wetting front is much smaller than that after the movement which may be due to repetition of wet and dry on the hot surface before the wetting front movement. The heat flux during the wetting time would be equal to that when the wetting front just moves. It is interesting that the magnitude of the peak heat flux decreases with increasing radial position.

3.2. Maximum heat flux in boiling curve

Quench cooling is particularly a complex phenomenon because different boiling modes occur simultaneously at different spatial positions relative to the wetting front. For this reason, it is useful to discuss the heat flux distribution with reference to corresponding boiling curves.

Fig. 3 represents the surface temperature and heat flux distribution in the radial direction along with a video image captured during the wetting front movement. The surface temperature, heat flux and the wetting front position are for 4.3 s after the first impingement of the jet. The picture can be divided into three regions: (a) no visible boiling ($r = 0$–12 mm), (b) vigorous boiling heat transfer ($r = 12$–18 mm) and (c) dry region ($r = 18$–45 mm). The region with no visible boiling activity is most likely single phase convection near the center with the onset to nucleation boiling beginning a little upstream of the vigorous boiling region in the zone marked (2).

The maximum heat flux point in the boiling curve traditionally represents the boundary between nucleation boiling and transition boiling. In Fig. 3 the maximum heat flux point appears at a radial position of 13.6 mm (≈14 mm), which is just inside the vigorous boiling region. As mentioned above, the region with $r = 10$–12 mm

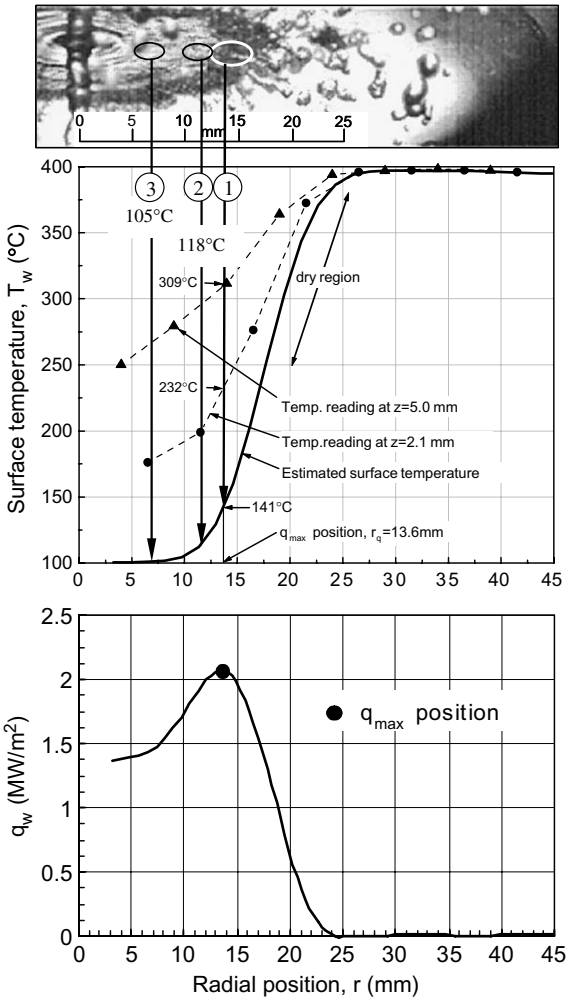

Fig. 3. Regimes of boiling and maximum heat flux during wetting front propagation (Steel: $T_b = 400$ °C, $\Delta T_{sub} = 50$ K, $u = 3$ m/s, $t = 4.3$ s).

belongs to the no visible boiling region but since the surface temperature is very high it is expected that nucleate boiling occurs but bubbles collapse quickly due to the high sub-cooling and consequently no vigorous boiling is observed. Thus in terms of the different modes of heat transfer the image in Fig. 3 may be interpreted as (i) single phase convection (0–10 mm) (ii) nucleation boiling (10–14 mm), (iii) transition boiling (14–18 mm) and (iv) single phase convection to vapor phase plus radiation (18–47 mm).

The surface temperatures and heat fluxes determined from the inverse solution are consistent with this interpretation. In the single phase convection region the surface temperature is close to the saturation point. For example at the position marked (3) in Fig. 3 the superheat is about 5 K, which is reasonable for single phase forced convection heat transfer. At the point (2) the surface superheat has increased to 18 K and heat flux increases monotonically with radial position towards the maximum, which is consistent with nucleation boiling in subcooled forced convection. At the maximum heat flux point, the surface superheat is 41 K. This again is higher than typical values for saturated nucleate pool boiling but reasonable for jet impingement with a subcooled liquid. In the dry region the surface temperature climbs rapidly from about 250 °C to the block initial temperature of 400 °C and the heat flux becomes very small.

Since the wetting front moves outwards in the radial direction each point on the surface will experience different boiling modes at different times depending on its position relative to the wetting front. This is apparent in Fig. 4 where cooling curves for individual points on the surface are plotted as boiling curves. The curves can be divided into four regions: single-phase convection, nucleation boiling, transition boiling and film boiling. The maximum heat flux serves as the boundary between nucleation boiling and transition boiling. It may be observed from Fig. 4 that for each boiling mode, the heat flux is generally greater for smaller radial positions. This may be due to a greater heat transfer enhancement from forced convection closer to the impingement zone and a tendency for the coolant temperature to rise with increasing radial position.

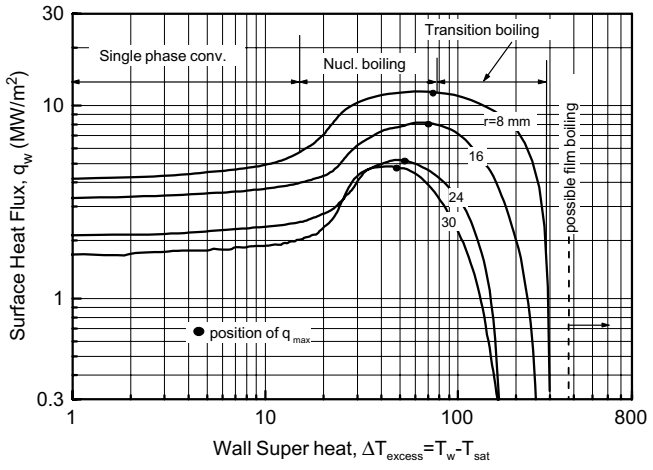

Fig. 4. Position of maximum heat flux in the regimes of boiling curve (Copper: $T_b = 400$ °C, $\Delta T_{sub} = 80$ K, $u = 15$ m/s).

The most important finding from the Fig. 4 is the surface temperature when the maximum heat flux occurs (i.e. T_w at q_{max}). When the maximum heat flux happens the surface temperature is 150–180 °C (for $r = 8$–30 mm according to this figure where $T_b = 400$ °C, $\Delta T_{sub} = 80$ K, $u = 15$ m/s). This temperature is always within a certain range for any radial position and any experimental condition. It is found that for most of the conditions (shown in the Table 1), the range of the surface temperature when the maximum heat flux occurs is (120–200) °C. It is also found from the present study that the T_w at q_{max} increases with the increase of liquid sub-cooling which is a general trend of boiling but still this change of T_w always falls within the range of 120–200 °C. Temperatures within this range are higher than the surface temperature required for saturated nucleate boiling in pool boiling.

3.3. Movement of maximum heat flux point

The mechanism for triggering the movement of the wetting front has still not been clarified [20]. Nevertheless, in general it is found that the commencement of the movement of the wetting front corresponds approximately to the appearance of the moving peak in the heat flux curve. For some conditions the maximum heat flux seems to appear slightly after the first visible observation of wetting front movement, but for the case in Fig. 2 these events are almost simultaneous.

The commencement of movement of the wetting front is also accompanied by visible and audible changes in the flow phenomena. Generally the boiling sound becomes loudest as the wetting front begins moving and liquid droplets are splashed away from the surface at a steep angle. Much vapor is generated due to rapid phase change associated with the maximum heat flux condition and the sound results from nucleate and transition boiling. These phenomena continue as the maximum heat flux point moves across the surface.

The mechanism that determines the speed of the wetting front also has not been clarified yet but it is likely that both heat flux and surface temperature play direct or indirect roles. To draw an analogy from steady state CHF experiments, CHF has been considered a boiling crisis where the 'dry out' point begins to occur at the outer edge of the heater [7]. In the present experiment we have a situation that appears similar where the boiling reaches a crisis point (maximum heat flux) just upstream of the wetting front. Beyond the wetting front the heater surface seems to be dry. Thus we may expect that in quenching experiments, rapid generation of vapor associated with the maximum heat flux will play an important role in the hydrodynamics to determine the movement or the position of the wetting front.

From the thermal perspective, the maximum heat flux also makes a direct contribution to the thermal conditions

of the surface ahead of the wetting front. Heat is transferred in the negative radial direction through the solid to the high heat flux zone. Thus the rate at which the solid surface is cooled in front of the wetting zone is a function of the solid thermal properties and the heat flux distribution within the wetted region. This is an important consideration since Fig. 4 indicates that the changes in boiling modes are connected to similar surface superheats for different radial positions.

Whatever the precise mechanism, it is likely that the wetting front shifts its position to keep a balance between the rate at which the solid side supplies heat and some hydrodynamic limitations of the liquid side to extract heat. The balance point itself may be due to a combination of hydrodynamic and thermal effects.

3.4. Effect of radial position on maximum heat flux

Fig. 5(a) compares a well-known relation for critical heat flux (CHF), q_c developed by Monde et al. [21] with present results for the maximum heat flux, q_{max} as a function of radial position. In this figure the heavy solid line (q_c) should be compared with the data having the symbols of circles (both solid and hollow). Two different characteristics as shown in the Fig. 5(a) is presented by region: I ($r_q = 5$–11 mm) with hollow symbols and region: II ($r_q = 11$–25 mm) with solid symbols. For a radial position less than about 11 mm (denoted as region I), the maximum heat flux decreases gradually with increasing r_q. In the region II, q_{max} also decreases more rapidly and the slope of this curve on the log-log plot is similar to that of the Monde prediction [21]. This suggests that there may be a connection between the mechanism for deciding the maximum heat flux in the present experiments and the CHF for steady-state experiments.

Wolf et al. [7] suggested that the decrease in CHF with increasing heater size is the result of poorer convection heat transfer further from the impingement region of the jet. However, from a different angle, Monde [22] was able to explain the decrease in CHF with heater diameter in terms of an overall heat balance and a hydrodynamic stability model by Haramura and Katto [23]. If the diameter (D) of the heater is large in comparison to the diameter of the jet, the relation derived by Monde [22] suggests the critical heat flux will be approximately proportional to $D^{-2/3}$ for saturated conditions. This is in accord with much experimental data for saturated impinging jet CHF. Monde [21] extended the flow model to account for jet subcooling showing that the subcooled CHF is an even stronger function of the heater diameter since the liquid becomes heated towards the saturation point as it flows in the radial direction. As shown in Fig. 5(a) the maximum heat flux in the present study is approximately proportional to $(r_q)^{-1}$ in the region II.

A general observation for the present quenching experiment is that the vigorous boiling region increases in area

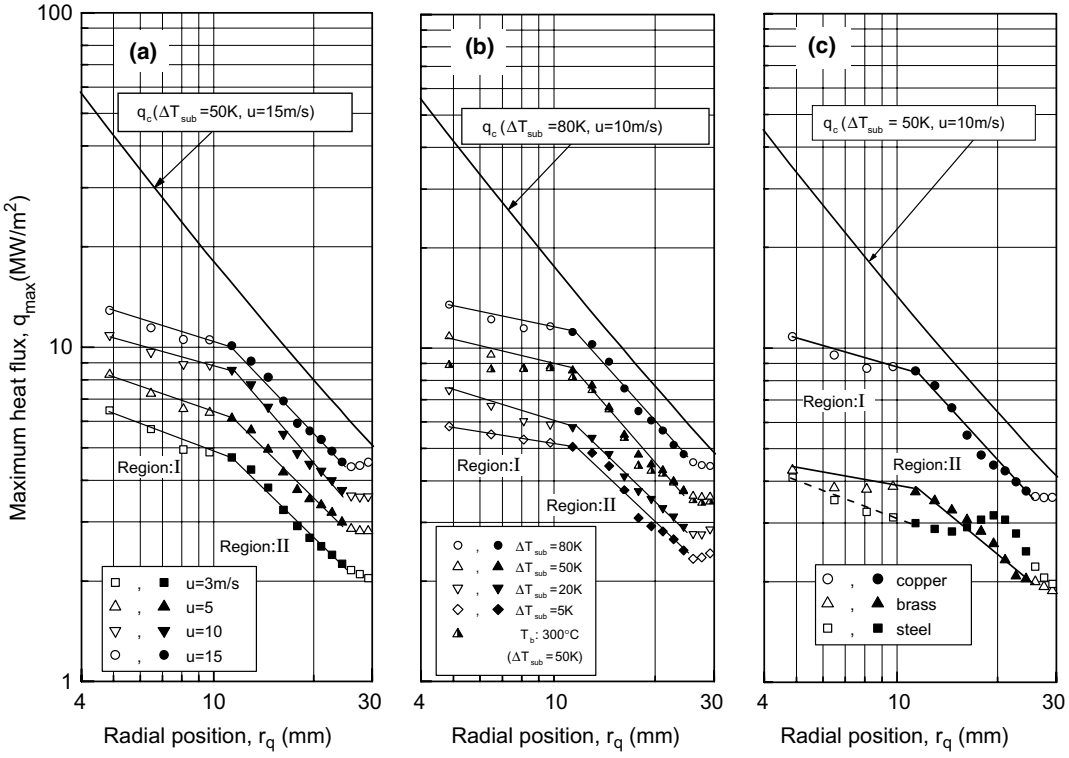

Fig. 5. Variation of critical and maximum heat flux with radial position for different (a) jet velocities (Cu, $T_b = 400$ °C, $\Delta T_{sub} = 50$ K), (b) subcoolings (Cu, $T_b = 400$ °C, $u = 10$ m/s) and (c) materials ($T_b = 400$ °C, $\Delta T_{sub} = 50$ K, $u = 10$ m/s). The solid symbols indicate Region II where the trend is similar to the CHF equation result, q_c.

as the wetting front moves outward in the radial direction. This is the result of the greater circumference and also an increasing width of the boiling region. The effect is evident in Fig. 2 where the heat flux distribution near the peak becomes broader and flatter as the peak moves outward in the radial direction. Thus a balance between supply of coolant and increasing available surface area is certainly a possible explanation for the decrease in maximum heat flux with increasing radial position shown in Fig. 5(a)–(c).

It is a little difficult to explain the change in character of the curves at around $r_q = 11$ mm (the border of regions I and II) in Fig. 5(a). All data in the figure are from the parallel flow region of the jet since this region starts around 2 jet diameters downstream of the stagnation point [7]. However, it is worth noting that this changing point in Fig. 5(a)–(c) corresponds approximately to the point where the developing boundary layer will reach the free surface if the flow is assumed laminar [24].

3.5. Effect of initial block temperature on maximum heat flux

Generally it is found that the effect of the initial block temperature on maximum heat flux is small. A comparison of the right half solid upward triangles with the hollow and full solid upward triangles in Fig. 5(b) is a typical example of the effect. The half solid triangles are for an initial temperature of 300 °C while the hollow and full solid triangles are for an initial temperature of 400 °C. For both cases, the subcooling and velocity are 50 K and 10 m/s respectively. In this particular case the largest differences appear at the smaller radial position where the heat flux is slightly higher for the higher initial temperature.

The main effect of the initial block temperature is on the time it takes to reach the maximum heat flux. This is consistent with the observation that the maximum heat flux usually occurs when the surface temperature is in the range 120–200 °C. A higher initial temperature means it takes longer time for the block to cool down to bring the surface temperature within this range.

While there may be a weak correlation between the initial temperature and maximum heat flux, in the correlation proposed in the present study we have assumed that q_{max} is independent of T_b.

3.6. Effect of block material on maximum heat flux

One of the most surprising findings in the present study is the effect of the solid material on the maximum heat flux. This is in contrast to critical heat flux for steady experiment, which has been found to be independent of the heater material. Fig. 5(c) gives a typical example of the effect of block material on the maximum heat flux. The data are for an initial temperature of 400 °C, a subcooling of 50 K and a jet velocity of 10 m/s. All three materials were given the same surface treatment and were plated with gold. It should be noted, however, that in spite of precautions, some oxidation and surface aging could be observed on each of the surfaces after many experiments. Nonetheless it is expected that the effects shown reflect the influence of the thermal properties of the bulk material rather than the surface condition or properties of oxidation.

Among three materials, copper shows the highest value of maximum heat flux, which is more than two times that of steel whose value is the minimum. Copper, brass and steel show a similar trend up to the radial position $r = 15$ mm. In the region $r = 15$–25 mm the trend of maximum heat flux with radial position is similar for copper and brass. However, for steel the maximum heat flux rises to reach a local peak at $r_q = 20$ mm and then falls again. This peculiarity for steel was observed for all experimental conditions.

Differences in thermal conductivity of the block material may be the key factor responsible for the higher maximum heat flux for copper than steel or brass. Copper has a thermal conductivity, λ of about 380 W/mK, which is over three times that of brass ($\lambda = 112$ W/mK) and ten times that of steel ($\lambda = 37.8$ W/mK). The basic trend is that the maximum heat flux increases with increasing thermal conductivity (or diffusivity) but not in direct proportion as may be deduced from Fig. 5(c).

In terms of the temperature distribution within the solid, quenching results in localized cooling near the surface for steel in contrast to copper/brass where the entire heated test piece quickly feels the effect of the maximum heat flux on the surface. It may be that this difference is partly responsible for the peculiar effect of radial position on q_{max} for steel. From video images it could be observed that after the wetting front starts moving in the radial direction it proceeds to the circumference without any further delay at any position for copper and brass. In the case of steel, however, at around the radial position 15–20 mm, the wetting front movement appears to suddenly become slower and then after almost stopping, the wetting velocity gradually increases and the front reaches to the end of the test piece. This behavior seems to suggest a hydrodynamic effect that perhaps was not obvious in the cases of copper and brass due to the strong influence of vigorous boiling on the flow behavior both upstream and downstream of the maximum heat flux point.

From Fig. 5(c) it is clear that brass and steel have closely comparable magnitude of maximum heat flux value but the nature of the change in maximum heat flux with radial position is most similar between copper and brass. For this reason we have not included the data for steel in the present proposed correlation for q_{max} together with copper and brass.

3.7. Effect of jet velocity on maximum heat flux

The variation of q_{max} with jet velocity has been presented in Fig. 6 for three different radial positions. Effect of velocity on q_{max} has been also shown in Fig. 5(a). Maximum heat flux increases gradually with increasing jet velocity. The jet velocity directly affects the flow rate of

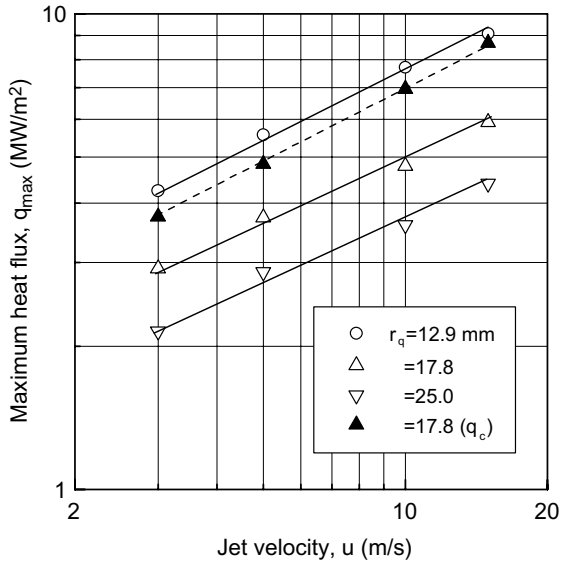

Fig. 6. Variation of maximum heat flux with jet velocity for different radial positions ($T_b = 400$ °C, $\Delta T_{sub} = 50$ K).

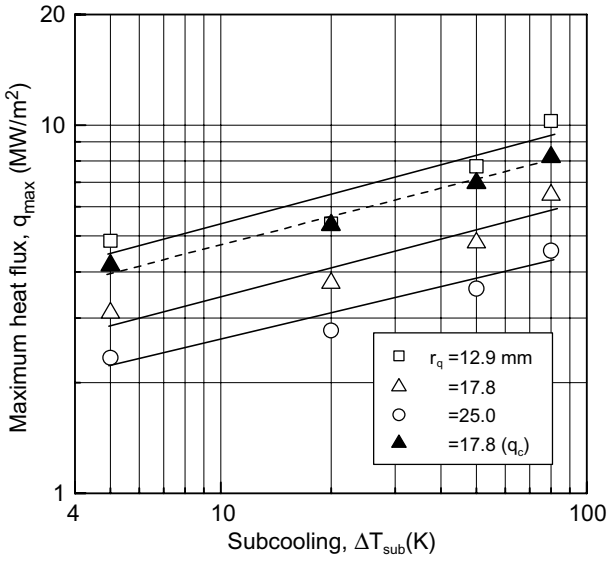

Fig. 7. Variation of maximum heat flux with subcooling for different radial positions ($T_b = 400$ °C, $u = 10$ m/s).

coolant to the test surface and has a strong bearing on convection heat transfer and the fluid hydrodynamics. If the flow model proposed by Monde [21] is applicable in the vicinity of the maximum heat flux point then the velocity directly affects the flow rate of coolant to the film of liquid on the surface. For V-regime (the regime where jet velocity is very important for critical heat flux) steady-state CHF, Monde [22] found that the critical heat flux is proportional to $u^{1/3}$ for saturated jets and the correlation proposed by Monde [21] suggests that the exponent should increase with greater subcooling. In the Fig. 6, a comparison also has been made between maximum heat flux and critical heat flux with the variation of jet velocity. The symbol of solid upper triangle is for q_c at radial position of 17.8 mm and the hollow triangle is for q_{max} at the same radial position. A similar trend of q_c and q_{max} with the variation of jet velocity has been observed from this figure.

3.8. Effect of subcooling on maximum heat flux

Fig. 5(b) also represents the variation of maximum heat flux with radial position for different subcoolings. With the increase of subcooling the maximum heat flux increases significantly. For reference, the estimated critical heat flux, q_c (for $\Delta T_{sub} = 80$ K, $u = 10$ m/s) is also included in Fig. 5(b).

Fig. 7 represents the variation of q_{max} with ΔT_{sub} for three different radial positions which are within the region II. Here q_{max} increases with subcooling. Higher subcooling increases the thermal potential between the solid and the impinged liquid which results in higher q_{max}. A similar trend has been observed for all experimental conditions. Comparison of q_{max} (hollow upward triangle) and q_c (solid upward triangle) with the variation of subcoolings for a particular radial position ($r = 17.8$ mm) has been also shown in the Fig. 7. One important finding from this figure is that the maximum heat flux has similar trend of critical heat flux with subcoolings.

3.9. Causes for difference between critical and maximum heat flux

As shown in the Fig. 5(a–c) the value of maximum heat flux, q_{max} is always smaller than the critical heat flux, q_c for any radial position. The rate of decrease of q_{max} with radial position is similar with that of q_c in the region $r_q = 11$–25 mm. In this region the difference between q_c and q_{max} is smaller than the region with smaller radial position. Many factors may be responsible for making this difference.

However, an important clue can be found in Fig. 5(c). In this figure, for the same jet velocity and subcooling the maximum heat flux is quite different depending on the solid material. This demonstrates that in contrast to critical heat flux, the thermal properties of solid material have a significant effect on the maximum heat flux during quenching. In particular the material with lower thermal conductivity have a lower maximum heat flux and the results for copper are closest to q_c. This is strong evidence that the thermal properties of the material place a limit on the maximum attainable heat flux during quenching. In other words there is a limit to the maximum rate at which the solid side can supply its stored heat to the surface. This limit is not present for steady-state CHF experiments where in contrast an external source or direct heating provides a constant supply of heat to the heater surface.

3.10. Influence of limitations of the inverse solution procedure

It should be mentioned that it is a little difficult to alternatively explain the large difference between the result for

copper and steel in Fig. 5(c) by a diminishing accuracy for the inverse solution comparing copper and steel. Fig. 3 includes the actual measured temperature at a depth of 2.1 mm. From this figure it can be seen that the sensors detected about 65% of the change from initial temperature at the surface. For copper under similar conditions the sensors at the first depth detected over 80% of the change in surface temperature. This change is much larger than the noise in the thermocouple reading, which was estimated to be less than 0.1 K. For the cases in Figs. 3 and 5(c) the velocity of the q_{max} point in the region II was about 2 to 4 mm/s for all materials. It is considered that this is slow enough so that the thermocouple response time is not a significant problem in this region. Also the penetration depth of the thermal wave is great enough to be detected easily by the sensors for all materials. Under similar conditions, numerical simulations [19] suggest the inverse solution should be quite accurate for all these materials.

The inverse solution result itself should be interpreted as an average over time and space. The time resolution cannot be greater than the response time of the sensors (about 0.1 s) or the time required for a thermal wave to penetrate to a depth of 5.0 mm (0.2 s for steel and 0.02 s for copper). The space resolution for the inverse solution is also limited to about 6.0 mm. Therefore the results for maximum heat flux are best understood as an average in space over about 6.0 mm.

According to Woodfield et al. [19] when the width of the high heat flux region is smaller than the pitch between the positions of two consecutive thermocouples, the inverse solution under-predicts the q_{max} value. This may help to explain why in the central region, less than about $r_q = 11$ mm, q_{max} was determined to even further from q_c. Near the central area the boiling region is narrow and as the wetting front moves outwards it becomes wider [14]. The boiling region in the central area ($r = 10$ mm) is about 2 mm wide and this value at $r = 25$ mm is about 5.5 mm (Brass, $T_b = 300$ °C, $\Delta T_{sub} = 50$ K, $u = 5$ m/s). The distance between two thermocouples beneath the test surface of the present study is approximately 5 mm. Therefore, near the center, as the width of the maximum heat flux region is smaller than pitch between consecutive thermocouples, the maximum heat flux in the central region is estimated to be lower than the actual value. This increases the difference between q_{max} and q_c. On the other hand, further from the centre, the boiling region (the region of maximum heat flux) is wider than that of thermocouples gap which prevents the under prediction of q_{max} from the inverse solution. For this reason, q_{max} is more accurate for greater radial positions.

Furthermore, the response of thermocouples might play a role for under predicting the value of q_{max} in the region I. The drop of temperatures with time is higher in smaller radial position than that of larger radial position. The thermocouples might not cope with this faster drop of temperature which results in decrease of accuracy of maximum heat flux estimation in smaller radial position. The wetting front velocity in the region I is much higher than that of the region II. This higher velocity might be responsible for under predicting the q_{max} value. But due to slow wetting front velocity this has not happened in the region II. The developed correlation and the focus of study in the present investigation belong to the region II and the estimation accuracy of the parameters in this region is high from all points of view.

3.11. Correlation for maximum heat flux

As discussed earlier, during quenching the solid material cannot supply enough heat to the liquid which has the consequence that q_{max} is always smaller than q_c. q_{max} in the present study is the maximum heat flux from transient experiments and q_c is the critical heat flux from steady state experiments conducted by Monde et al. [21]. In well designed steady state experiments due to the external power source the solid material can supply heat to the surface as if the solid conductivity is infinite. Therefore, it may be assumed that if it would possible to conduct transient experiments with material having infinite conductivity, then the q_{max} and q_c values should be close together. On the basis of this interpretation, a correlation of q_{max} is proposed in this study starting from the following critical heat flux correlation developed by Monde et al. [21] for subcooled impinging jets at steady state conditions:

$$\frac{q_c}{q_{co}} = \frac{1+\sqrt{1+4CJa}}{2} \tag{1}$$

$$\frac{q_{co}}{\rho_g h_{fg} u} = 0.221(\rho_l/\rho_g)^{0.645}\left[\frac{2\sigma}{\rho_l u^2 (D-d)}\right]^{0.343}(1+D/d)^{-0.364} \tag{2}$$

$$C = \frac{0.95(d/D)^2(1+D/d)^{0.364}}{(\rho_l/\rho_g)^{0.43}[2\sigma/\rho_l u^2(D-d)]^{0.343}} \tag{3}$$

where, $D = 2r_q$ for the present study.

In the present investigation, experimentation has been conducted for three material copper, brass and steel. Due to different characteristics of steel as discussed in the Section 3.6, it is not included together with copper and brass in the proposed correlation. Furthermore, Fig. 5(a)–(c) reveal that q_{max} data can be categorized into two regions, region I ($r_q = 5$–11 mm) and region II ($r_q = 11$–25 mm). The trend of region II is similar with that of q_c.

Fig. 5(a)–(c) highlight the similarity between q_c and q_{max} as a function of r_q. It is also found that q_{max} shows the same trend as q_c expressed by Eqs. (1)–(3) when plotted as a function of jet velocity, u, and jet subcooling, ΔT_{sub}. In all cases q_{max} is smaller than q_c by a factor which differs depending on the solid material properties. Therefore we propose that the key difference between q_{max} in transient experiments and q_c in steady state experiments can be accounted for by a correction involving thermal properties of material. Here, the steady state condition is replaced by a combination of material thermal properties $\sqrt{\rho c \lambda}$ which plays an important role in transient heat transfer when two semi infinite bodies suddenly comes into contact. In

addition, from the previous discussion it is desirable that q_{max} approaches q_c as the thermal conductivity of the solid approaches infinity. On the basis of this interpretation a relation between q_{max} and q_c is proposed by Eq. (4).

$$\frac{q_{max}}{q_c} = 1 - 5.5\sqrt{\frac{(\rho c\lambda)_l}{(\rho c\lambda)_s}} \tag{4}$$

The coefficient 5.5 in Eq. (4) has been estimated using least mean squares method from the data of q_{max} of the present experiment. Eq. (4) is valid in the region II. Fig. 8 represents the agreement between the data for q_{max} of copper and brass and the correlation. Most of the data is within ±30% of the proposed correlation. The few data points that fall outside of this range (inside the dotted area) mostly correspond to conditions where the wetting front starts moving almost immediately after the jet first strikes the surface. In general, when the jet velocity and jet subcooling are high the data trends to be more scattered, but even in such cases most of the data is within the ±30% range. The scatter in Fig. 8 may be due partly to the time response of the thermocouples during very rapid cooling.

The block initial temperature, T_b in some cases was found to have a weak influence on q_{max} which was not included in the proposed correlation. Therefore, T_b may contribute to the scattering of data. Also, the proposed correlation in the present study has been initiated from the correlation of critical heat flux, q_c of Monde et al. [21] which itself has ±20% scattering [25].

In Fig. 9, the proposed correlation is compared with data for steel. The scattering is very high which might be due to the different characteristics of steel relative to copper and brass as described in the Section 3.8. Future study should clarify the behavior of q_{max} for steel and the q_{max} in region I for copper and brass.

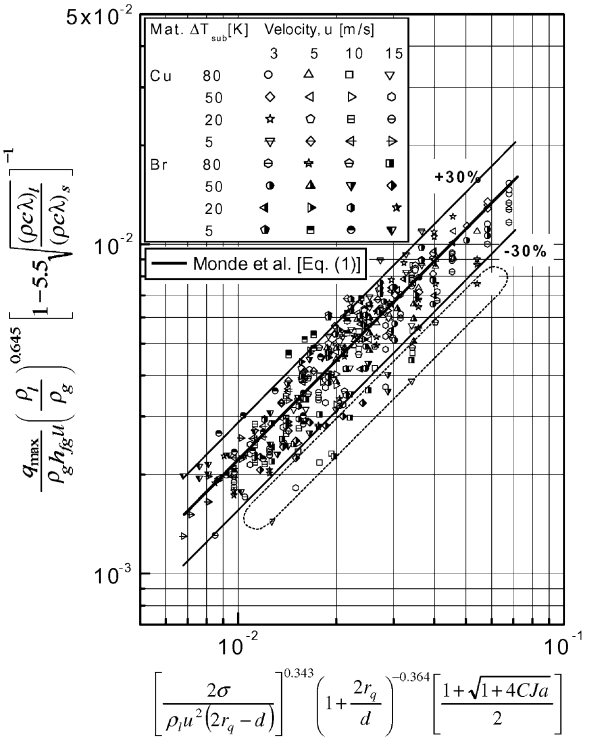

Fig. 8. Comparison of q_{max} data for copper and brass with the proposed correlation (for region II).

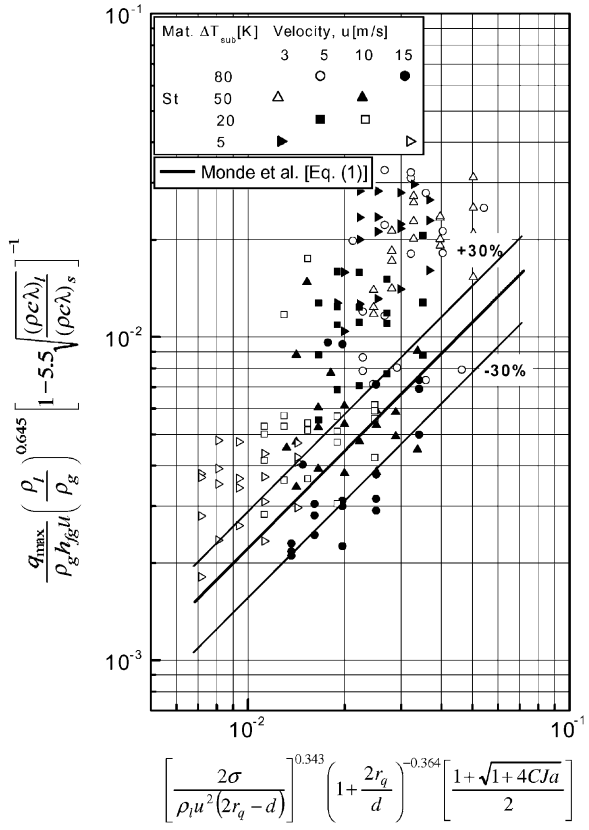

Fig. 9. Comparison of q_{max} data for steel with the proposed correlation (for region II).

4. Conclusions

In the present study emphasis has been given to find out the parameters that govern maximum heat flux during quenching. With the combination of key parameters a correlation for maximum heat flux has been proposed. At present the fundamental accomplishments from this study are summarized as:

1. The maximum heat flux always occurs during the movement of the wetting front. During this movement the position of the maximum heat flux also moves from the center towards the circumference. During this radial movement, the maximum heat flux is found to occur within the visible boiling region for any experimental condition.
2. Stable nucleate boiling is established at the position of maximum heat flux.
3. Maximum heat flux, q_{max} is a strong function of jet velocity and thermal properties of block material. It is also a moderate function of jet subcooling. q_{max} is a weaker function of the block initial temperature, T_b.

4. The maximum heat flux in the region II for copper and brass can be predicted with an accuracy of ±30% by Eq. (4) together with Eq. (1).

Acknowledgements

The 'Grant-in-Aid for Scientific Research (C), 2005', partial support from JSPS and the advice of Y. Mitsutake are acknowledged.

Appendix A

The inverse solution procedure is implemented by fitting the thermocouple readings to equations in the form of Eq. (A.1) for each depth using a least-squares method to determine the coefficients $P_{j,k}^{(n)}$.

$$f(\tau,\gamma,\zeta_n)=\sum_{j=0}^{N_j}J_0(m_j\gamma)\cdot\sum_{k=0}^{N}\frac{P_{j,k}^{(n)}\cdot\tau^{k/2}}{\Gamma(k/2+1)}\quad\text{at } n=1,2 \tag{A.1}$$

where, $f(\tau,\gamma,\zeta_n)$ is temperature variation function on plane $\zeta=\zeta_n$ beneath the surface The unsteady heat conduction equation and Eq. (A.1) are transformed to the Laplace domain and then solved. Using an approximate inverse Laplace transform procedure the solutions for the surface temperature and heat flux are obtained explicitly in the form of Eqs. (A.2) and (A.3) respectively.

$$\theta_w(\tau,\gamma)=\sum_{j=0}^{N_j}\sum_{\ell=-1}^{N}G_{j,\ell}^{(1,2)}\cdot\frac{\tau^{\ell/2}}{\Gamma(\ell/2+1)}\cdot J_0(m_j\gamma)-\sum_{j=0}^{N_j}\sum_{\ell=-1}^{N}G_{j,\ell}^{(2,1)}\cdot\frac{\tau^{\ell/2}}{\Gamma(\ell/2+1)}\cdot J_0(m_j\gamma) \tag{A.2}$$

$$\Phi_w(\tau,\gamma)=\sum_{j=0}^{N_j}\sum_{\ell=-1}^{N}H_{j,\ell}^{(1,2)}\cdot\frac{\tau^{\ell/2}}{\Gamma(\ell/2+1)}\cdot J_0(m_j\gamma)-\sum_{j=0}^{N_j}\sum_{\ell=-1}^{N}H_{j,\ell}^{(2,1)}\cdot\frac{\tau^{\ell/2}}{\Gamma(\ell/2+1)}\cdot J_0(m_j\gamma) \tag{A.3}$$

where, J_0 is Bessel function, τ is non-dimensional time, ζ is non-dimensional distance in axial direction, γ is non-dimensional distance in radial direction of the block and m_j is eigen value. The coefficients $G_{j,l}^{(m,n)}$ and $H_{j,l}^{(m,n)}$, the mathematical derivation and practical implementation of the inverse solution have been discussed in details in [17–19].

References

[1] J.D. Bernardin, C.J. Stebbins, I. Mudawar, Mapping of impact and heat transfer regimes of water drops impinging on a polished surface, Int. J. Heat Mass Transfer 40 (2) (1997) 247–267.
[2] D.E. Hall, F.P. Incropera, R. Viskanta, Jet impingement boiling from a circular free-surface jet during quenching: Part 2—two-phase jet, ASME J. Heat Transfer 123 (4) (2001) 911–917.
[3] J.D. Bernardin, I. Mudawar, The Leidenfrost point: experimental study and assessment of existing models, ASME J. Heat Transfer 121 (4) (1999) 894–903.
[4] M. Monde, Y. Katto, Burnout in a high heat flux boiling system with an impinging jet, Int. J. Heat Mass Transfer 21 (1978) 295–305.
[5] P.L. Woodfield, M. Monde, A.K. Mozumder, The possibility of homogeneous nucleation boiling during transient liquid/solid contact in a jet impingement quench cooling system, Thermal Sci. Eng. 12 (4) (2004) 39–40.
[6] P.L. Woodfield, M. Monde, A.K. Mozumder, Observations of high temperature impinging-jet boiling phenomena, Int. J. Heat Mass Transfer 48 (2005) 2032–2041.
[7] D.H. Wolf, F.P. Incropera, R. Viskanta, Jet impingement boiling, Adv. Heat Transfer 23 (1993) 1–132.
[8] S. Ishigai, S. Nakanishi, T. Ochi, Boiling heat transfer for a plane water jet impinging on a hot surface, in: Proceedings of the 6th International Heat Transfer Conference, 1978, pp. 445–450.
[9] Y. Barnea, E. Elias, Flow and heat transfer regimes during quenching of hot surfaces, Int. J. Heat Mass Transfer 37 (1994) 1441–1453.
[10] S.S. Dua, C.L. Tien, An experimental investigation of falling-film rewetting, Int. J. Heat Mass Transfer 21 (1978) 955–965.
[11] J. Filipovic, F.P. Incropera, R. Viskanta, Quenching phenomena associated with a water wall jet: 1. Transient hydrodynamic and thermal conditions, Exper. Heat Transfer 8 (1995) 97–117.
[12] S. Kumagai, S. Suzuki, Y. Sano, M. Kawazoe, Transient cooling of a hot metal slab by an impingement jet with boiling heat transfer, in: ASME/JSME Thermal Engineering Conference, vol. 2, 1995.
[13] E. Hall, P. Incropera, R. Viskanta, Jet impingement boiling from a circular free-surface jet during quenching: Part 1—single-phase jet, ASME J. Heat Transfer 123 (2001) 901–910.
[14] J. Hammad, Y. Mitsutake, M. Monde, Movement of maximum heat flux and wetting front during quenching of hot cylindrical block, Int. J. Thermal Sci. 43 (2004) 743–752.
[15] J. Hammad, M. Monde, Y. Mitsutake, Characteristics of heat transfer and wetting front during quenching by jet impingement, Thermal Sci. Eng. 12 (1) (2004) 19–26.
[16] T. Ochi, S. Nakanishi, M. Kaji, S. Ishigai, Cooling of a hot plate with an impinging circular water jet, in: T. Nejat Veziroglu, A.E. Bergles (Eds.), Multiphase-Phase Flow and Heat Transfer III, Part A: Fundamentals, Elsevier, Amsterdam, 1984, pp. 671–681.
[17] M. Monde, H. Arima, W. Liu, Y. Mitsutake, J.A. Hammad, An analytical solution for two-dimensional inverse heat conduction problems using Laplace transform, Int. J. Heat Mass Transfer 46 (2003) 2135–2148.
[18] J. Hammad, M. Monde, Y. Mitsutake, H. Arima, Determination of surface temperature and heat flux using inverse solution for two dimensional heat conduction, Thermal Sci. Eng. 10 (2) (2002) 17–26.
[19] P.L. Woodfield, M. Monde, Y. Mitsutake, Implementation of an analytical two-dimensional inverse heat conduction technique to practical problems, Int. J. Heat Mass Transfer 49 (2006) 187–197.
[20] A.K. Mozumder, M. Monde, P.L. Woodfield, Delay of wetting propagation during jet impingement quenching for a high temperature surface, Int. J. Heat Mass Transfer 48 (2005) 5395–5407.
[21] M. Monde, K. Kitajima, T. Inoue, Y. Mitsutake, Critical heat flux in a forced convection subcooled boiling with an impinging jet, Heat Transfer 7 (1994) 515–520.
[22] M. Monde, Critical heat flux in saturated forced convective boiling on a heated disk with an impinging jet, Warme Stoffubertr. 19 (1985) 205–209.
[23] Y. Haramura, Y. Katto, A new hydrodynamic model of critical heat flux, applicable widely to both pool and forced convection boiling on submerged bodies in saturated liquids, Int. J. Heat Mass Transfer 26 (1983) 389–398.
[24] E.J. Watson, The radial spread of a liquid jet over a horizontal plane, J. Fluid Mech. 20 (1964) 481–499.
[25] M. Monde, Critical heat flux in saturated forced convection boiling on a heated disk with one or multiple impinging jets, Trends Heat, Mass Momentum Transfer 1 (1991) 33–44.